

Negative ions in single and dual frequency capacitively coupled fluorocarbon plasmas

G A Curley¹, D Marić^{1,3}, J-P Booth¹, C S Corr^{1,2}, P Chabert¹ and J Guillon¹

¹ LPTP Ecole Polytechnique, 91128 Palaiseau Cedex, France

² PRL, Australian National University, Canberra, Australia

E-mail: curley@lptp.polytechnique.fr

Received 31 July 2006, in final form 12 December 2006

Published 31 January 2007

Online at stacks.iop.org/PSST/16/S87

Abstract

We have studied charged particle densities and fluxes in a customized industrial etch reactor, running in Ar/O₂/c-C₄F₈ gas mixtures at pressures in the region of 50 mTorr and driven by 2 and 27 MHz RF power, either separately or simultaneously. Independent control of ion flux and ion energy is the aim of using dual frequency plasmas. However, little experimental data exists regarding the charged particle dynamics in complex industrial gas mixtures. Negative ions could play an important role in this type of plasma. The presence of negative ions will modify the positive ion flux arriving at a surface, and they may even reach the surface and participate in etching. We have measured the electron density using a microwave hairpin resonator and the positive ion flux with a RF biased ion flux probe. The ratio of these two quantities, which depends on the negative ion fractions and other factors, is seen to vary strongly with gas chemistry, giving evidence for the presence of negative ions. Our results indicate high electronegativity for high c-C₄F₈ flow rates. We have also examined the effect of varying the 2 and 27.12 MHz RF powers on both the electron density and the positive ion flux. This allows us to estimate the effect of varying power on the negative ion density. In addition, ultra-violet cavity ring-down spectroscopy was used to measure the F⁻ density directly (Booth *et al* 2006 *Appl. Phys. Lett.* **88** 151502). This optical measurement was compared with the probe technique.

1. Introduction

Capacitively coupled low-pressure plasmas with dual frequency excitation have become standard in industrial dielectric etching, as they allow for the independent control of both the mean energy and flux of positive ions striking the substrate [2, 3]. Typically, argon is used as a buffer gas to reach the required pressure and to facilitate high positive ion densities. Fluorocarbon gases such as c-C₄F₈ and CF₄ [4] are often used as precursors to more reactive species which participate in the etching process. Due to dissociative attachment processes, the latter gases represent an efficient source for the creation of negative fluorine ions. It has been shown that the fluorine negative ion (F⁻) is expected to be the dominant negative ion in C₄F₈ and CF₄ plasmas [5–7].

³ Permanent address: Institute of Physics Belgrade, POB 68, 11080 Zemun, Serbia.

The presence of negative ions has been considered a problem in plasma processing, as it can lead to a significant reduction in the positive ion flux to the substrate [8–10], to particulate formation [11, 12] and to instabilities [13]. Furthermore, negative ions can influence the plasma chemistry, through fast ion–neutral and ion–ion reactions. If they can reach the substrate, they could participate in etching and may alleviate profile charging effects [14].

Numerous diagnostic techniques have been applied to detect negative ions in plasmas. Laser induced photodetachment followed by the detection of electrons by a Langmuir probe or microwave resonance has been shown to be successful [5–7, 15–17]. However, due to their aggressive reactive environments and large RF potentials, these techniques are difficult to implement in industrial etch reactors. They may also cause perturbations and their results are difficult to put on an absolute scale. Measurement of the optical

absorption below the photodetachment threshold (364.5 nm for F^-) appears to be more adapted to the direct measurement of the negative ion density in such environments.

However, the very low photodetachment cross section limits standard optical methods to very high F^- densities [18]. By allowing very small absorbances to be measured, cavity ring-down spectroscopy (CRDS) is a promising technique but also more challenging as the mirrors available at the necessary short wavelengths have poor overall reflectivities. Quandt *et al* [19] were the first to use the CRDS to detect negative ions by measuring the density of H^- . Recently, we reported the detection of negative fluorine ions using CRDS [1].

Chabert *et al* [20] used a two probe technique (planar probe and cylindrical probe), with a model developed by Sheridan [21], to determine negative ion fractions, $\alpha = n_-/n_e$. The advantages of using probes to measure α lies in the experimentally simple setup and the localized results. However, one needs a good model for the positive ion flux to the probe when negative ions are present and an accurate measurement of the electron current or density. In addition one usually wishes to perform such measurements in reactive and possibly magnetized plasmas where problems due to probe contamination and anisotropy may arise.

In this paper, we have used a technique similar to Chabert *et al* [20] to estimate the negative ion fraction, α , in the centre of the plasma. However, there are some notable changes. Firstly, instead of using a Langmuir probe, we determine n_e directly using the hairpin probe technique introduced by Stenzel [22] and recently examined by Piejak *et al* [23]. The use of this probe in capacitive RF plasmas has since been examined [24–26]. Secondly, we have used an RF biased planar probe [27, 28] to measure the ion flux. The principal advantage of this technique is its ability to function well even under conditions where an insulating layer has been deposited on the probe surface. The combination of the hairpin probe and the RF biased planar probe is particularly well adapted to a large range of plasma configurations and, more specifically, to reactive capacitive plasmas.

In this work, our aim was to evaluate the use of these probes in measuring, in the context of a dual frequency plasma with complex gas mixtures, the electron densities and positive ion fluxes and thereby deducing both the negative ion fractions and negative ion densities. It was also our aim to compare the CRDS and probe measurements under similar conditions.

Section 2 of this paper briefly describes the diagnostic techniques used, with particular attention to their implementation in our reactor. Section 3 outlines some of the principal probe results. In section 4 we present our CRDS measurements. Finally, in section 5 we use the results from the probes to estimate α and to compare with the CRDS measurements of F^- .

2. Experiment

The experimental setup is shown in figure 1. The plasma was formed in a modified commercial dual frequency capacitively-coupled dielectric etch reactor, designed for 200 mm industrial wafer processing using fluorocarbon gases. The capacitive discharge is driven between two electrodes spaced 25 mm apart. The upper (silicon) electrode is grounded. RF power

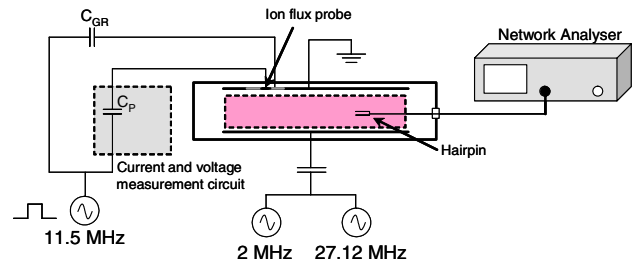


Figure 1. Simplified schematic of the ion flux and hairpin probe experimental setup. C_{GR} and C_P are the coupling capacitors for the guard ring and probe respectively.

(This figure is in colour only in the electronic version)

at frequencies of 2 and 27 MHz is supplied to the lower electrode, which is covered by an electrostatically clamped 200 mm silicon wafer. A flow of helium assures the thermal contact between the wafer and the electrode. The plasma is confined radially by a stack of five quartz rings spaced several millimetres apart. Gases used in this study were Ar, C_4F_8 and O_2 which enter through a showerhead configuration in the upper electrode and exit through the gaps in the confinement rings before being pumped out of the reactor. The gas pressure inside the rings was typically around 50 mTorr with input powers of 250 W for the single frequency case and 500 W for the dual frequency (2 MHz = 250 W, 27 MHz = 250 W). Although we did perform measurements using CF_4 , they are not presented in this paper for the sake of clarity and space. Those results will be presented in a future paper.

The diagnostics used in this work are well adapted to the aggressive environment of reactive processing plasmas. The positive ion flux was measured using an ion flux probe and the electron density with a microwave ‘hairpin’ resonator. The negative fluorine ion, F^- , density was measured directly by high-sensitivity CRDS.

2.1. Ion flux probe

The ion current to the upper (grounded) electrode was measured using an RF biased planar ion flux probe [27, 28]. The probe (stainless steel, diameter = 5 mm) is installed coplanar with the upper electrode and is surrounded by a guard ring (outer diameter = 15 mm, inner diameter = 5.1 mm) (see figure 1). The guard ring is independently biased to the same potential as the probe. An RF (11.5 MHz) modulated pulse is applied to the probe across a coupling capacitor and becomes negatively self-biased in the presence of a plasma. Following termination of the pulse, the initial discharge rate of the coupling capacitor (and likewise its transient current) is directly related to the ion flux. A voltage and current measurement circuit was built to facilitate this. We can then trace a current–voltage (I – V) curve in the ion current saturation region.

The I – V curves are fitted to obtain the ion current, floating potential and effective ‘tail’ temperature of the electron energy distribution function (EEDF). We found that a Maxwellian EEDF did not fit the data adequately in all the cases. A satisfactory fitting could be achieved by a function that allows the EEDF to vary between Maxwellian and Druyvesteyn like

forms:

$$I = I_0 \left[1 - m(V - V_f) - \exp \frac{(V - V_f) - k(V - V_f)^2}{T_e} \right], \quad (1)$$

where V is the potential on the probe surface, V_f is the steady floating potential, T_e is the electron tail temperature and m is the slope of the I - V curve in the saturation region. The k parameter weights the $(V - V_f)^2$ term, and increases as the EEDF becomes more truncated, i.e. $k = 0$ describes the Maxwellian only case.

This probe is deposition tolerant, which is critical for the diagnostics of processing plasmas. Any deposited layer becomes an effective capacitance in series with the probe and the coupling capacitor and therefore reduces the discharge rate. However, it will not change the transient current through the capacitor [28] at a given voltage.

2.2. Hairpin resonator probe

A quarter-wave microwave resonator ('hairpin' resonator), similar to that used by Piejak *et al* [23, 24], was used to measure the electron density. A short piece of tungsten wire (diameter = 0.125 mm) was bent into a U-shape about 4 cm long and microwave power, swept in frequency, is coupled to it by means of an induction loop supplied via a coaxial cable (diameter = 2 mm). The coax was built in-house using glass as the dielectric between the centre and outer conductors. This allows it to survive the high temperatures (>500 K), which common coax cables cannot. Also, due to the aggressive nature of our plasma (chemical and ion etching, strong RF fluctuations) we have built probes in which the coax cable is fully protected by a glass (quartz) tube. The hairpin is attached to this tube and is electrically floating, allowing it to follow the plasma potential [24–26]. This way, we minimize plasma perturbations and the effects of uncompensated RF fluctuations across the sheath that forms around the hairpin wires. The reflected power was observed using a network analyser to obtain the resonant frequency. The probe is centred between the electrodes. On the radial axis it is about one third of the way into the plasma, which can confidently be considered to be uniform over the wafer surface. Due to resonances in the various coax cables, we took differential spectra of the hairpin signal to eliminate as much as possible any undesirable resonant peaks. In practice, we subtract the 'plasma ON' signal from the 'plasma OFF' signal, where the plasma off resonance peak is measured immediately after the plasma is switched off. This helps to compensate for any changes in vacuum resonance due to heating of the hairpin wires by the plasma. The principal advantages of using the hairpin probe include the direct measurement of n_e , self-calibration (from the vacuum resonance) and minimal error due to the thermal expansion and fluorocarbon deposition. Sheath effects would result in a lower electron density measurement [23], but this was found not to play a significant role in our results.

2.3. Cavity ring-down spectroscopy

Cavity ring-down spectroscopy was used to measure the absorption spectrum of the plasma. Details of our CRDS setup are presented in [1]. The optical cavity, centred in

the plasma, both axially and radially, consisted of two high reflectivity mirrors (Layertec, $R > 99.8\%$ in the 340–380 nm range), with 1 m radius of curvature mounted 1.6 m apart on flexible bellows at the end of extension tubes. The laser beam was produced by a dye laser with frequency doubling (Sirah, using Styryl 8 or Pyridine 2 dyes), itself being pumped by a frequency-doubled Nd-YAG (yttrium aluminium garnet) (532 nm at 10 Hz). Typical laser energies were several tenths of a millijoule in the range 340–380 nm, with a pulse duration of 9 ns. The laser beam quality was improved by a spatial filter consisting of a 50 mm focal length lens (L1) and a 50 μ m pinhole (PH) and then injected into the cavity with a 60 mm focal length lens (L2). This improved the spectrum's reproducibility and base line stability. The light escaping the cavity was detected by a photomultiplier tube fitted with an UV bandpass filter to exclude visible light. The exiting light is observed to decay exponentially with a time constant known as the ring-down time τ :

$$\tau = \frac{L}{c[1 - R(\lambda)]}, \quad (2)$$

where L is the cavity length, c is the speed of light and R is the mirror reflectivity. An absorbing medium reduces the ring-down time of the cavity. A LabVIEW™ routine was developed to control the data acquisition sequence and determine the ring-down time for each laser shot in real time. Depending on the laser wavelength, typical ring-down times between 2 and 4 μ s were obtained. The plasma was switched on for 5 s and switched off for 5 s and the ring-down times for both 'plasma on' and 'plasma off' were calculated for at least 30 on/off cycles. In this way the noise (error on the mean) could be reduced to the equivalent of 10^{-6} per single pass. The absorption (per single pass) of the plasma as a function of wavelength, $A(\lambda)$, was calculated from the difference in ring-down times for both plasma on, τ_{on} , and plasma off, τ_{off} :

$$A(\lambda) = \frac{L}{c} \left[\frac{1}{\tau_{\text{on}}(\lambda)} - \frac{1}{\tau_{\text{off}}(\lambda)} \right]. \quad (3)$$

The F^- density was estimated by fitting the observed absorption spectrum to the function:

$$A'(\lambda) = \sigma(\lambda)n_{F^-}L + B, \quad (4)$$

where $\sigma(\lambda)$ is the F^- photodetachment cross section at a given wavelength [29], n_{F^-} is the F^- density, L is the plasma length and B is a constant background.

3. Ion flux probe and hairpin results

The electron density, n_e , and the positive ion flux, Γ_i (current density, J_i) were measured in both single (27 MHz) and dual (2 and 27 MHz) frequency capacitive RF plasmas. The dependence of measured quantities on gas chemistry and on input power were investigated in Ar/C₄F₈/O₂ and Ar/CF₄/O₂ gas mixtures.

3.1. Effects of gas mixture composition

Argon flow was kept constant (160 sccm, sccm—standard cubic centimetre per minute), while flows of fluorocarbon gas

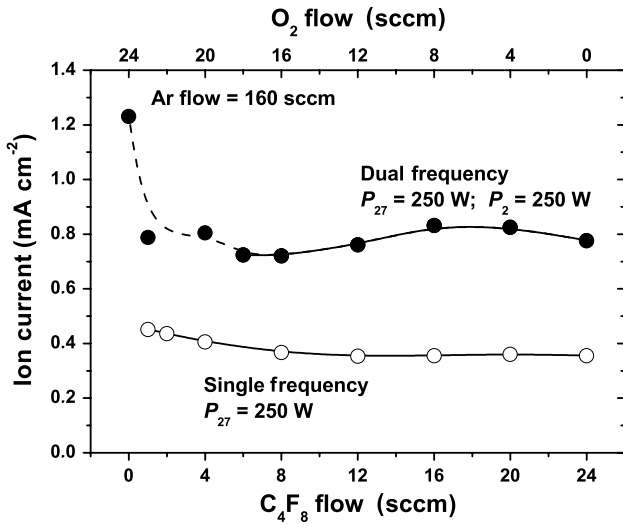


Figure 2. Ion current densities in Ar/C₄F₈/O₂ single and dual frequency discharges showing dependence on C₄F₈ and O₂ flows at fixed argon flow (160 sccm) with a total pressure of around 50 mTorr.

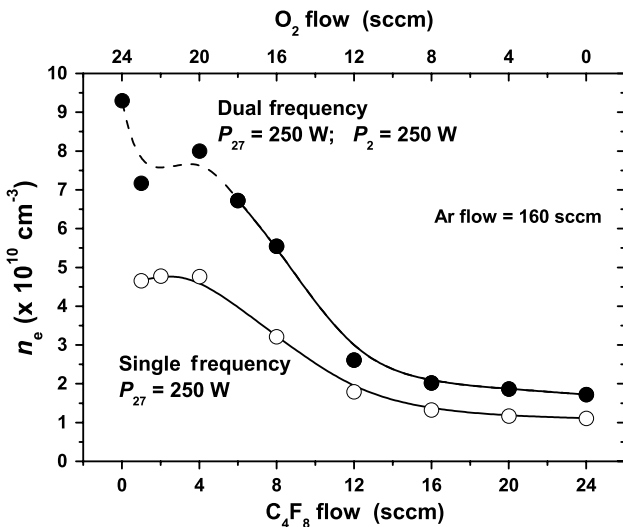


Figure 3. Electron densities under similar conditions to figure 2.

and oxygen were varied, but keeping the total flow of both the gases fixed (O₂ + C₄F₈ = 24 sccm, O₂ + CF₄ = 40 sccm). Pressure in the reactor was approximately 50 mTorr (6.6 Pa). Both high and low frequency input powers are kept at 250 W.

Figure 2 shows that the ion current density is reduced in both single and dual frequency plasmas when C₄F₈ is added, although this is less pronounced in the single frequency case. For certain dual frequency plasma conditions, Ar/O₂ plasma and small flows of C₄F₈, it was difficult to achieve stable conditions. This is indicated by the dashed line. Addition of oxygen to Ar/C₄F₈ plasma does not seem to have a significant effect on the ion flux.

The electron density in the single frequency case is unaffected until more than 4 sccm of C₄F₈ is added, at which point it falls rapidly (figure 3). In dual frequency, plasma instabilities were observed on the left-hand side of the curve; however the electron density seems to have the same trend with the addition of C₄F₈. Our previous measurements with similar

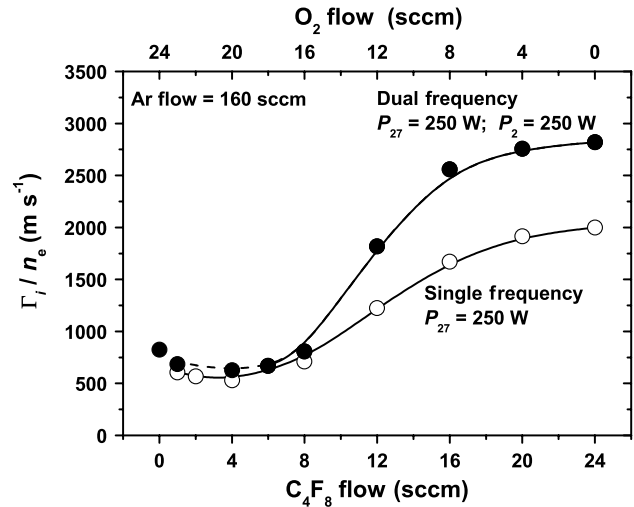
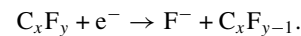


Figure 4. Positive ion flux to electron density ratios using data from figures 2 and 3.

gas flow ratios confirm this [25]. Addition of O₂ leads to a small gradual increase in electron density.

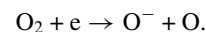
Generally, the ratio of ion flux, Γ_i , to electron density, n_e increases when negative ions are present, so it is interesting to analyse this ratio's dependence on plasma chemistry. In electropositive plasmas this ratio should be equal to the product $h_1 \cdot v_B$, where v_B is the ion velocity at the sheath edge (Bohm velocity) and h_1 is the edge-to-centre plasma density ratio. Assuming a collisional model [30], we expect values of $h_1 \sim 0.2$ and $\Gamma_i/n_e \sim 700 \text{ m s}^{-1}$, for our discharge conditions. However, in electronegative plasmas this ratio is expected to increase with a higher negative ion fraction, both in the non-collisional [20] and collisional [21] case.

Figure 4 shows the effect of the gas mixture composition on the ion flux to electron density ratio. At higher C₄F₈ flows, Γ_i/n_e significantly increases for both single and dual frequency excitation, indicating a high density of negative ions, probably F⁻. The most probable mechanism for the production of fluorine negative ions is dissociative attachment of fluorocarbon radicals:



As typical etching recipes fall on the right-hand side of figure 4, this region is the most important for closer investigation.

In the range of very low C₄F₈/O₂ flow ratios, observed instabilities enable us to make only a crude estimation of Γ_i/n_e value. As the gas mixture approaches the Ar/O₂ case, there is a slight increase in the ion flux to electron density ratio. Previous measurements [25] showed a much more pronounced increase of the ratio in this region. This trend suggests the possible presence of negative oxygen ions, probably created through dissociative attachment:



The ratio passes through a minimum when the gas composition is ~ 4 sccm of C₄F₈ and ~ 20 sccm of O₂, approaching a value close to the estimated electropositive

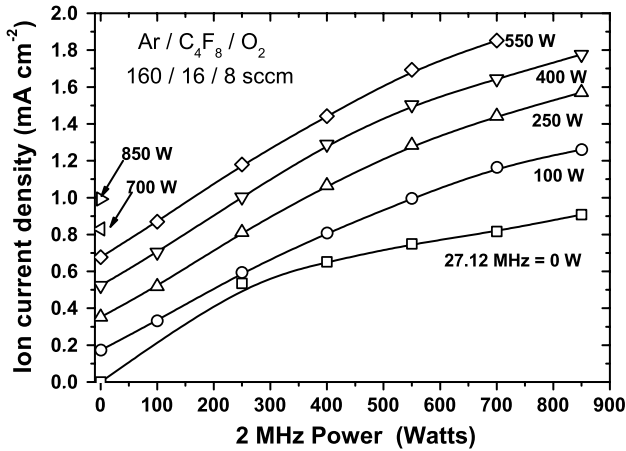


Figure 5. Ion current densities as a function of 2 MHz power at fixed 27 MHz power levels.

value. This suggests that the $\text{Ar}/\text{C}_4\text{F}_8$ plasma contains F^- , the Ar/O_2 plasma contains O^- and that no negative ions are present in the region where the ratio has its minimum. The destruction of negative ion precursors is a likely explanation for this. The C_xF_y precursors for F^- are destroyed, possibly forming species such as CO , COF and CO_2 , therefore also removing the precursors to O^- .

3.2. Effects of input power

Ion flux as a function of 2 MHz powers at fixed 27 MHz power levels is presented in figure 5. We have selected to present results for a gas mixture composition closest to the actual industrial conditions— $\text{Ar}/\text{C}_4\text{F}_8/\text{O}_2$ flows equal to 160/16/8 sccm.

It can be seen that the efficient decoupling of ion production from 2 MHz power is not achieved, although 27 MHz power is somewhat more efficient at increasing the ion flux, especially at higher 2 MHz powers. In fact, one would expect the 2 MHz to contribute to the ionization at lower powers. We expect a more efficient decoupling at higher powers, compared with those that we could achieve in our reactor.

Figure 6 shows the ion flux to electron density ratio. For a single frequency plasma ($P_{2\text{MHz}} = 0$) the ratio does not show any significant dependence on the 27 MHz power. Increasing the 2 MHz power results in a small initial increase in the ion flux to electron density ratio. Considering the relationship between this ratio and the negative ion fraction, this may suggest an increase in the negative ion density with a 2 MHz power. However, there is little change in its value at higher powers. Increasing the 27 MHz power leads to an initial decrease in the ratio, and then the effect saturates.

4. Cavity ring-down results

Probe measurements indicated that, for conditions comparable to those used for dielectric etching, a significant negative ion density can be expected. Therefore, we tested these predictions by direct measurement of the F^- ion density.

Figure 7 shows the F^- absorption profile versus laser wavelength for a single and dual frequency $\text{Ar}/\text{C}_4\text{F}_8/\text{O}_2$

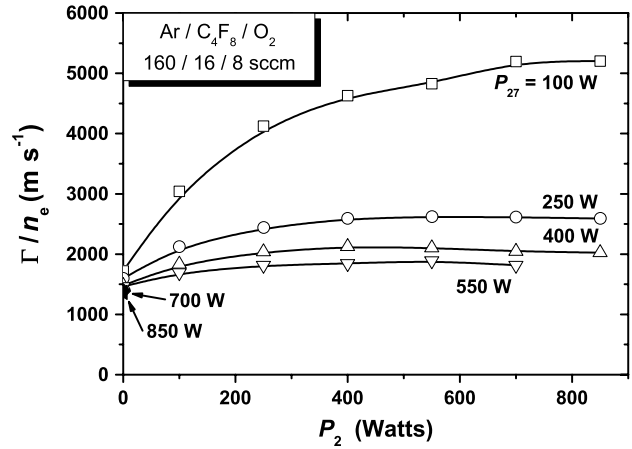


Figure 6. Ion flux to electron density ratios as a function of 2 MHz power at fixed 27 MHz power levels.

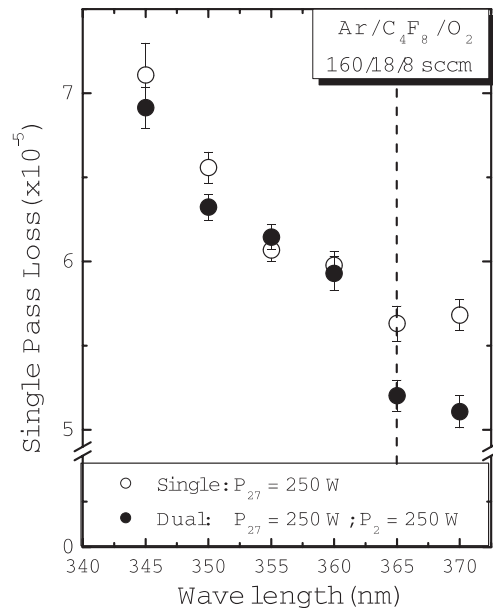


Figure 7. Effective single pass loss as a function of laser wavelength in an $\text{Ar}/\text{C}_4\text{F}_8/\text{O}_2$ gas mixture for single and dual frequency excitation.

(160/18/8 sccm) discharge. Input powers are 250 W for the single frequency (27 MHz) and 250 W (27 MHz) + 250 W (2 MHz) for the dual frequency. Above the photodetachment threshold of 364.5 nm, the base line is flat, indicating that the increase in absorption below this value is due to F^- . A fit to the experimental data estimates a F^- density of $1.7 \times 10^{11} \text{ cm}^{-3}$ for a single frequency case and $2 \times 10^{11} \text{ cm}^{-3}$ in the dual frequency. The error bars represent the statistical uncertainty in the mean value of the absorbance determined at each point due to variations in the ring-down time and do not include any estimation of systematic errors. The error is largest at the wavelength extrema, where the mirror reflectivity is the lowest.

The negative ion densities obtained here are in good agreement with previous observations for C_4F_8 containing plasmas [6, 15].

These results appear to contradict the prediction of Georgieva *et al* [31] that, in the presence of the low frequency

RF power (2 MHz), the relatively light F^- ions would be accelerated towards the electrode by the strong electric fields, whereas the heavier CF_3^- ions would respond less to the low frequency fields and become the main negative ion. On the contrary, our results show even higher fluorine negative ion densities in the dual frequency plasma. However, more recent calculations [32], taking into account our geometry and gas pressure, suggest that a significant F^- deconfinement should not occur until a higher 2 MHz RF power than used here is applied.

5. Estimation of negative ion fraction

We have used a model developed by Sheridan and co-workers [8, 21] to estimate negative ion fractions (α) in the plasma centre from both the ion flux probe and the hairpin resonator probe results. In these calculations, electron temperatures were estimated on the basis of the ion flux probe results ($T_e \sim 3$ eV for single frequency excitation and $T_e \sim 8$ eV for dual frequency).

Our measurement of T_e is from the tail of the EEDF so it must be noted that this may not be representative of the bulk electron temperature. The high T_e values in the dual frequency case are possibly overestimated if we consider them to be equal to the bulk temperature. However, this is currently our only means of estimating T_e . The results were plotted for electron to negative ion temperature ratios ($\gamma = T_e/T_-$) of 10 and 30. Indeed, the negative ion temperature is an elusive, yet fundamentally important, parameter in the calculation of α . The reason we chose 10 and 30 as example values is that they give α estimates that we believe are in a realistic range. Higher values of γ would give negative ion fractions of 100 and above. This choice will be discussed later in this section.

The application of the model involves first calculating the normalized ion flux, $\Gamma_{is}/(n_{e0}c_s)$, where Γ_{is} is the ion flux at the plasma sheath edge, n_{e0} is the centre electron density and c_s is the ion acoustic speed in the absence of negative ions ($\sqrt{kT_e/M_i}$). One must also determine the characteristic collisional parameter (δ) of the plasma. The collisional parameter characterizes the number of collisions that an ion experiences before leaving the plasma. It is defined as L/λ_{eff} , where L is the plasma length and λ_{eff} is an effective mean free path $= c_s/v_p$. Here c_s is the electropositive Bohm velocity and v_p is the collision frequency for momentum transfer. The normalized ion flux values are then associated with different values of α for a fixed δ .

Negative ion fractions calculated from the data in figure 4 are shown in figure 8(a) for the dual frequency plasma and in figure 8(b) for the single frequency plasma.

The major error in determining α comes from the fact that we do not know γ or more explicitly, we do not know the negative ion temperature. Given this, we will never be able to correctly estimate the absolute value of alpha from probes only. On top of this, there is the fact that the technique is inaccurate for alphas smaller than 2–3. This means that where alphas of 3 or less are estimated, one cannot guarantee the presence of significant numbers of negative ions. Error bars could be included to include the error in T_e , but we feel this to be unnecessary in the context of these graphs. The negative ion fraction varies greatly as a function of C_4F_8/O_2 flows and is

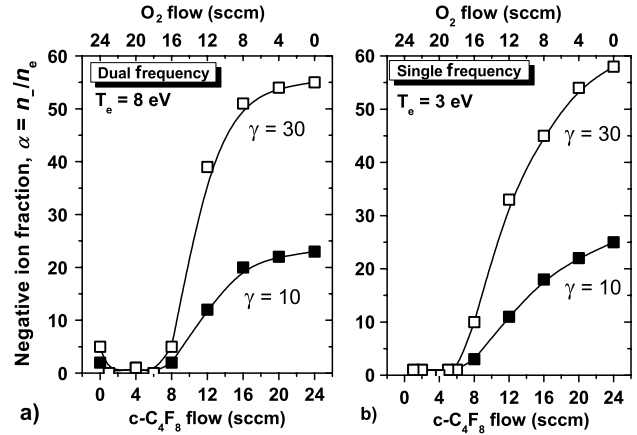


Figure 8. Estimated negative ion fractions as a function of C_4F_8 and O_2 flows ($p = 50$ mTorr), for (a) dual and (b) single frequency discharges.

almost identical for both single and dual frequency excitation. This is in spite of the fact that the ratios in figure 4 are not identical. This is due to the normalization process whereby different values of T_e were used. Ion flux to electron density ratios by themselves are therefore not enough to give a full picture of the plasma electronegativity.

For the mixture $Ar/C_4F_8/O_2 = 160/18/8$ sccm, the negative ion fractions estimated by combining the CRDS and hairpin probe results are of the order of ~ 10 , assuming F^- is the dominant negative ion. This agrees well with the negative ion fractions from the probe technique if we take $\gamma = 10$. This is another reason for our choices of γ earlier. This estimate for γ is interesting to note, as measuring negative ion temperature is very often not possible and not reliable. The fact that T_- must be much greater than room temperature to allow for the observed Γ_i/n_e ratios gives evidence for strong negative ion heating mechanisms. Combining optical measurements of F^- with probe measurements to deduce α has in fact brought us to a reliable means of estimating negative ion temperatures.

6. Conclusion

We have presented measurements of the electron density and the ion flux in both single (27 MHz) and dual frequency (2 + 27 MHz) fluorocarbon plasmas. The techniques that we used for measurements have been proven to be very reliable even in aggressive environments typical of processing plasmas. We monitored the positive ion flux to electron density ratio in order to identify conditions where negative ions can be very important. Flows of the gases were varied over a broad range, while the discharge pressure was kept constant, so that we could avoid pressure induced variation in measured quantities. It has been shown that the Γ_i/n_e ratio varies strongly with gas chemistry and gives evidence for the presence of negative ions, especially in the range of importance for practical processing conditions.

The effects of input power variation on plasma properties have also been studied. The Γ_i/n_e ratio increases with increasing 2 MHz powers and decreases with increasing 27 MHz powers. Further studies will have to be undertaken to investigate this. Other factors could also be contributing to

these trends, such as an increase in the edge-to-centre electron density ratio, h_1 , caused by an increase in the sheath width (smaller plasma size) due to higher 2 MHz power.

F^- negative ion densities were measured by the direct observation of the weak continuum absorption below 364.5 nm due to photodetachment, using the cavity ring-down technique. The F^- densities in Ar/CF₄/O₂ and Ar/C₄F₈/O₂ plasmas were in the range 10^{11} cm^{-3} . The densities were not significantly different for single or dual frequency excitation.

Negative ion fractions have been estimated from the ion flux probe and hairpin resonant probe measurements, indicating that α is strongly dependent on plasma chemistry. For the conditions studied in this work it changes from 0 to ~ 20 , assuming a γ of ~ 10 . Comparison with the cavity ring-down results has shown that the two methods applied give α of the same order of magnitude when the electron temperature to negative ion temperature ratio is chosen to be of the order of 10. This has allowed us to confirm the existence of strong negative ion heating mechanisms and high negative ion temperatures.

Acknowledgment

The authors acknowledge financial support and donation of equipment from the Lam Research Corporation.

References

- [1] Booth J P, Corr C S, Curley G A, Jolly J and Guillon J 2006 *Appl. Phys. Lett.* **88** 151502
- [2] Goto H H, Lowe H D and Ohmi T 1992 *J. Vac. Sci. Technol. A* **10** 3048–54
- [3] Boyle P C, Ellingboe A R and Turner M M 2004 *J. Phys. D: Appl. Phys.* **37** 697–701
- [4] Lieberman M A and Lichtenberg A J 1994 *Principles of Plasma Discharges and Materials Processing* (New York: Wiley)
- [5] Kono A and Ohya Y 2000 *Japan. J. Appl. Phys. (Part 1 3A)* **39** 1365–8
- [6] Hebner G A and Abraham I C 2001 *J. Appl. Phys.* **90** 4929–37
- [7] Jauberteau J L, Meeusen G J, Haverlag M, Kroesen G M W and de Hoog F J 1989 *Appl. Phys. Lett.* **55** 2597–9
- [8] Sheridan T E, Chabert P and Boswell R W 1999 *Plasma Sources Sci. Technol.* **8** 457–62
- [9] Boyd R L F and Thompson J B 1959 *Proc. R. Soc. A* **252** 102
- [10] Braithwaite N S J and Allen J E 1988 *J. Phys. D: Appl. Phys.* **21** 1733–7
- [11] Choi S J and Kushner M J 1993 *J. Appl. Phys.* **74** 853
- [12] Howling A A, Sansonnens L, Dorier J L and Hollenstein C 1994 *J. Appl. Phys.* **75** 1340
- [13] Chabert P, Lichtenberg A J, Lieberman M A and Marakhtanov A M 2001 *Plasma Sources Sci. Technol.* **10** 478–89
- [14] Ohtake H and Samukava S 1996 *Appl. Phys. Lett.* **68** 2416
- [15] Kono A and Kato K 2000 *Appl. Phys. Lett.* **77** 495
- [16] Takada N, Hayashi D, Sasaki K and Kadota K 1997 *Japan. J. Appl. Phys. (Part 2)* **36** L1702
- [17] Bacal M 1993 *Plasma Sources Sci. Technol.* **2** 190–7
- [18] Nagai S, Sakai M, Furuhashi H, Kono A, Goto T and Uchida Y 1998 *IEEE J. Quantum Electron.* **34** 40–6
- [19] Quandt E, Kraemer I and Dobele H F 1999 *Europhys. Lett.* **45** 32
- [20] Chabert P, Sheridan T E, Boswell R W and Perrin J 1999 *Plasma Sources Sci. Technol.* **8** 561–6
- [21] Sheridan T E 1999 *J. Phys. D: Appl. Phys.* **32** 1761–7
- [22] Stenzel R L 1976 *Rev. Sci. Instrum.* **47** 603–7
- [23] Piejak R B, Godyak V A, Garner R, Alexandrovich B M and Sternberg N 2004 *J. Appl. Phys.* **95** 3785–91
- [24] Piejak R B, Al-Kuzee J and Braithwaite N S J 2005 *Plasma Sources Sci. Technol.* **14** 734–43
- [25] Curley G, Booth J P and Guillon J 2005 *Proc. 27th ICPIG (Eindhoven, Netherlands)* Article 08-230
- [26] Karkari S K and Ellingboe A R 2006 *Appl. Phys. Lett.* **88** 101501
- [27] Braithwaite N S J, Booth J P and Cunge G 1996 *Plasma Sources Sci. Technol.* **5** 677–84
- [28] Booth J P, Braithwaite N S J, Goodyear A and Barroy P 2000 *Rev. Sci. Instrum.* **71** 2722–7
- [29] Vacquié S, Gleizes A and Sabsabi M 1987 *Phys. Rev. A* **35** 1615–20
- [30] Godyak V A 1986 *Soviet Radio Frequency Discharge Research* (Falls Church, VA: Delphic Associates)
- [31] Georgieva V, Bogaerts A and Gijbels R 2003 *J. Appl. Phys.* **94** 3748–56
- [32] Georgieva V 2006 private communication